symmetry

MDPI

Article

Magnetic Structure of CoO

Ekkehard Krüger

Institut für Materialwissenschaft, Materialphysik, Universität Stuttgart, D-70569 Stuttgart, Germany; ekkehard.krueger@imw.uni-stuttgart.de

Abstract: The paper reports evidence that the multi-spin-axis magnetic structure proposed in 1964 by van Laar is realized in antiferromagnetic CoO. This tetragonal spin arrangement produces both the strong tetragonal and the weaker monoclinic distortion experimentally observed in this material. The monoclinic distortion is proposed to be a "monoclinic-like" distortion of the array of the oxygen atoms, comparable with the rhombohedral-like distortion of the oxygen atoms recently proposed to be present in NiO and MnO. The monoclinic-like distortion has no influence on the tetragonal magnetic structure, which is generated by a special nonadiabatic atomic-like motion of the electrons near the Fermi level. It is argued that it is this atomic-like motion that qualifies CoO to be a Mott insulator.

Keywords: CoO; antiferromagnetic eigenstate; magnetic groups; Mott insulator; atomic-like motion; non-adiabatic Heisenberg model; magnetic band; magnetic super band

Citation: Krüger, E. Magnetic Structure of CoO. *Symmetry* **2021**, *13*, 1513. https://doi.org/10.3390/sym13081513

Academic Editors: Raffaele Barretta and Vladimir A. Stephanovich

Received: 1 June 2021
Accepted: 13 August 2021
Published: 17 August 2021

1. Introduction

Cobalt monoxide is antiferromagnetic with the Néel temperature $T_N = 289$ K. Just as the other isomorphic transition-metal monoxides MnO, FeO, and NiO, it is a Mott insulator in both the paramagnetic and the antiferromagnetic phase. While above T_N, all the transition-metal monoxides possess the fcc structure $Fm3m = \Gamma_c^f O_h^5$ (225) (in parentheses we always give the number in the International Tables for Crystallography), CoO occupies a special position in the magnetic phase: the magnetic structures of MnO, FeO and NiO are known to be monoclinic base-centered [1–4], but the magnetic structure of CoO is not fully understood. Two different models of antiferromagnetic CoO are discussed in the literature: first, the non-collinear multi-spin-axis magnetic structure with tetragonal symmetry proposed in 1964 by van Laar [5] and, second, a collinear monoclinic structure similar to that of the other monoxides. The models can hardly be distinguished by neutron diffraction data or by reverse Monte Carlo refinements of these data [6]. They are considered as alternative structures or as structures coexisting in antiferromagnetic CoO [7]. The non-collinear structure is suggested by the marked tetragonal distortion of CoO accompanying the antiferromagnetic state, and a collinear structure could be associated with the additional small monoclinic deformation unambiguously detected in the antiferromagnetic phase of CoO [8].

1.1. Problem Statement

The group theoretical non-adiabatic Heisenberg model (NHM) [9] defines in narrow half-filled energy bands a strongly correlated nonadiabatic atomic-like motion not existing in the adiabatic system. In the nonadiabatic system, the electrons no longer follow adiabatically the nuclei and have a greater freedom of movement in a system adapted to symmetry of the crystal [9]. Any application of the NHM starts from a pure one electron band structure not taking into account correlation effects. The electronic correlation enters into the theory only by the postulates of the NHM. The band structure of paramagnetic CoO used in this paper is calculated by the FHI-aims ("Fritz Haber Institute ab initio molecular simulations") program using the density functional theory [10,11] to compute the total energy in the electronic ground state.

As is generally accepted, the antiferromagnetism and Mott insulation of the transition-metal monoxides MnO, NiO, CoO, and FeO are manifestations of strongly correlated electrons in narrow *d* bands [12–21]. However, the strongly correlated atomic-like motion emerging when we leave the adiabatic approximation, was not yet taken into consideration. The aim of the present paper and of three forgoing papers [22–24] on MnO and NiO is to fill this gap. In the present paper we show that, just as in MnO and in NiO, the non-adiabatic atomic-like motion defined within the NHM is evidently responsible for both the magnetic structure and the Mott insulation in CoO.

The NHM applies group theoretical methods to the exact non-adiabatic atomic-like motion of the electrons at the Fermi level. Thus, this model has clear limitations because group theoretical methods are not suited for the calculation of any matrix elements. For this purpose, we must represent the (highly complex) non-adiabatic localized states by atomic or Wannier functions. Such an "adiabatic approximation" of the non-adiabatic atomic-like motion should yield physically relevant results whenever an atomic-like motion occurs in the considered material, i.e., whenever the Bloch functions near the Fermi level possess a suitable symmetry. Thus, our results do not contradict but complement the proven concepts of correlation effects in narrow *d* bands cited above.

In addition, we will show that a shift of the Co atoms causes the stability of the antiferromagnetic state as well as a small "monoclinic-like" deformation of the array of the oxygen atoms. This monoclinic-like deformation is comparable to the rhombohedral-like distortion proposed to exist in antiferromagnetic MnO and NiO.

1.2. Organization of the Paper

In the following Section 2, the magnetic group of the multi-spin-axis structure is determined. Just as in NiO and MnO, a problem emerges in this context: a system invariant under the already reported [5,6] type IV Shubnikov magnetic group I_c4_1/acd given in Equation (1) cannot possess antiferromagnetic eigenstates. As shown in Section 3, for this reason, the crystal undergoes a marked tetragonal distortion reducing the symmetry initially defined by the group I_c4_1/acd. As demonstrated in Section 4, this tetragonal distortion evidently produces a monoclinic-like deformation of the array of the oxygen atoms in the deformed crystal.

In Section 5, the non-adiabatic Heisenberg model (NHM) shall be applied to the electronic ground state of CoO. In Section 5.1, we will show that the electrons of paramagnetic CoO may occupy an atomic-like state allowing the system to be a Mott insulator. Having in Section 2 determined the active magnetic group of antiferromagnetic CoO, we may apply the NHM to the antiferromagnetic state of CoO, too. In Section 5.2, we will determine the magnetic band related to the magnetic group of the antiferromagnetic state. The electrons may perform an atomic-like motion in the nonadiabatic system stabilizing the tetragonal non-collinear magnetic structure. In addition, this atomic-like motion allows the electron system to be Mott insulating.

2. Magnetic Group of the Antiferromagnetic State

The multi-spin-axis structure of CoO [5] is indicated in Figure 1a by red arrows. It is invariant under the space group $I4_1/acd$ (142) [5] and under the type IV Shubnikov magnetic group [6]:

$$I_c4_1/acd = I4_1/acd + \{K|\tfrac{1}{2}\tfrac{1}{2}0\}I4_1/acd, \tag{1}$$

where K denotes the anti-unitary operator of time-inversion. The unitary subgroup $I4_1/acd$ has the tetragonal body-centered Bravais lattice Γ_q^v and contains (besides the pure translations) sixteen elements that are expressible as products of the three generating elements

$$\{C_{4z}^+|\tfrac{1}{2}00\}, \{\sigma_{da}|\tfrac{1}{2}\tfrac{1}{2}0\}, \text{ and } \{I|000\}. \tag{2}$$

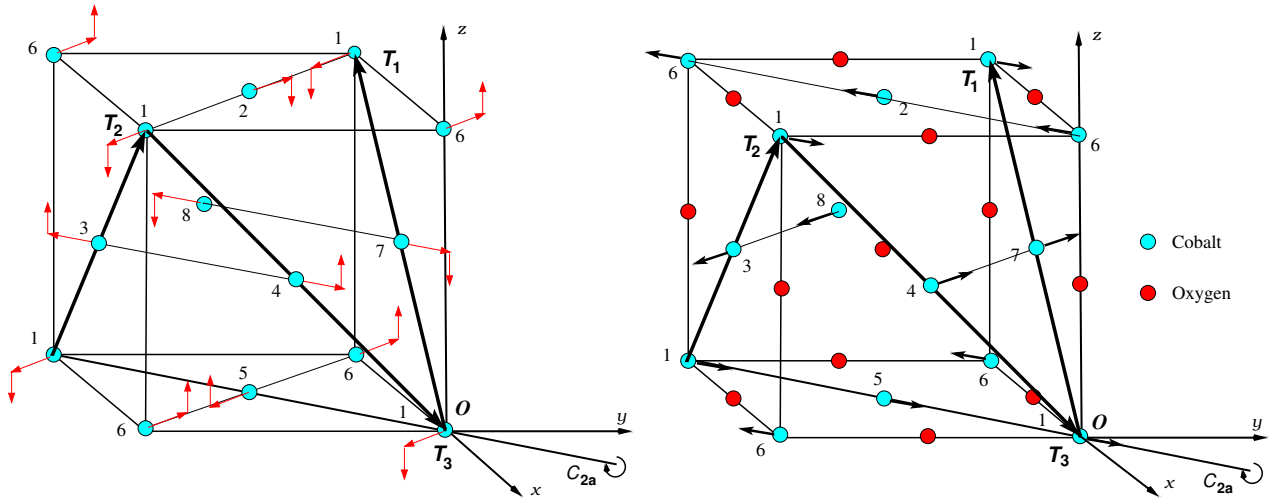

Figure 1. Antiferromagnetic CoO with the magnetic group M_{110} (Equation (14)) based on the tetragonal body-centered Bravais lattice Γ_q^v. The eight Co atoms in the unit cell are (arbitrarily) numbered from 1 to 8. The three vectors $\boldsymbol{T}_i$ are the basic translations of Γ_q^v. (**a**) Magnetic structure of CoO invariant under M_{110}. The O atoms are not shown. The red arrows denote two components of the magnetic moments at the Co atoms. The components parallel to the plain (001) lie in the $\pm(\boldsymbol{T}_1 + \boldsymbol{T}_3)$ or $\pm(\boldsymbol{T}_2 + \boldsymbol{T}_3)$ direction and are all of the same size, the other components in the $\pm z$ direction are also of the same size. The figure is consistent with Figure 3 of [5]. (**b**) Distortion of CoO invariant under M_{110}. The arrows denote the shifts of the Co atoms stabilizing the antiferromagnetic structure. The drawn shifts in the $\pm(\boldsymbol{T}_1 + \boldsymbol{T}_3)$ or $\pm(\boldsymbol{T}_2 + \boldsymbol{T}_3)$ direction form the only distortion of the antiferromagnetic lattice invariant under M_{110}. Any shift of the O atoms, on the other hand, cannot happen because it would destroy the symmetry of M_{110}.

We write the symmetry operations $\{R|\alpha\beta\gamma\}$ in the Seitz notation: R is a point group operation written with respect to the x, y, and z axes in Figure 1 and $\alpha\boldsymbol{T}_1 + \beta\boldsymbol{T}_2 + \gamma\boldsymbol{T}_3$ the subsequent translation [25], where the basis translations $\boldsymbol{T}_i$ are also defined in Figure 1. We write the point group operations R as defined in Section 1.4 of [25], here $R = E$ stands for the identity operation, $R = C_{4z}^+$ for the anti-clockwise rotation through 90° about the z axis, $R = I$ for the inversion, $R = C_{2a}$ for the rotation through 180° about the a axis as indicated in Figure 1, and $R = \sigma_{da}$ for the reflection IC_{2a}. Since the magnetic structure in Figure 1 (a) is invariant under the three generating elements 2 and under the anti-unitary element $\{K|\frac{1}{2}\frac{1}{2}0\}$, it is invariant under the complete magnetic group 1.

In what follows, the magnetic group I_c4_1/acd is referred to as M_{142} because the unitary subgroup $I4_1/acd$ bears the international number 142,

$$M_{142} = I4_1/acd + \{K|\tfrac{1}{2}\tfrac{1}{2}0\}I4_1/acd. \tag{3}$$

Table A1 lists the character tables of the single valued irreducible representations of $I4_1/acd$. In particular, the entry (a) below $\{K|000\}$ means that all the one-dimensional representations of $I4_1/acd$ follow Case (a) with respect to the gray magnetic group $I4_1/acd + \{K|000\}I4_1/acd$. Case (a) is defined by Equation (7.3.45) of [25], in the present case, the one-dimensional representations follow Case (a) because they are real. According to Condition 1 in [23], the antiferromagnetic state cannot be an eigenstate of a system invariant under M_{142} because $I4_1/acd$ does not possess at least one one-dimensional representation following Case (c) (as defined by Equation (7.3.47) of [25]).

These group-theoretical findings change drastically when we assume that the subgroup $I4_1/cd$ (110) of $I4_1/acd$ (142) is the unitary part of the magnetic group of antiferromagnetic CoO. $I4_1/cd$ contains one-half of the sixteen elements of $I4_1/acd$ (142) and may be defined by the generating elements

$$\{C_{4z}^+|\tfrac{1}{2}00\} \text{ and } \{\sigma_{da}|\tfrac{1}{2}\tfrac{1}{2}0\}, \tag{4}$$

see Table 3.7 of [25]. However, the origin used in the Tables of [25] for the space group $I4_1/cd$ (110) is different from the origin used in the present paper (and marked in Figure 1 by O). Thus, all the symmetry operations S_{BC} used in [25] for the group $I4_1/cd$ (110) must be transformed by $\{E|0\frac{1}{4}\frac{3}{4}\}$ into the symmetry operations S_{paper} used in this paper,

$$S_{paper} = \{E|0\tfrac{1}{4}\tfrac{3}{4}\}S_{BC}\{E|0\tfrac{1}{4}\tfrac{3}{4}\}^{-1}. \tag{5}$$

Just as the group $I4_1/acd$, the group $I4_1/cd$ has the tetragonal body-centered Bravais lattice Γ_q^v. From $I4_1/cd$ we may derive two magnetic groups, the type IV Shubnikov group

$$M_1 = I4_1/cd + \{K|\tfrac{1}{2}\tfrac{1}{2}0\}I4_1/cd \tag{6}$$

(with a black and white Bravais lattice), and the type III Shubnikov group

$$M_2 = I4_1/cd + \{KI|\tfrac{1}{2}\tfrac{1}{2}0\}I4_1/cd \tag{7}$$

(with an ordinary Bravais lattice), both leaving invariant the magnetic structure. The one-dimensional representations at point Z in Table A2 now follow both requirements (i) and (ii) of Condition 1 of [23] for the magnetic group M_2, but no one-dimensional representation of $I4_1/cd$ meets both requirements (i) and (ii) for M_1.

Thus, the type III Shubnikov group M_2 is the magnetic group of antiferromagnetic CoO because it allows the system to possess antiferromagnetic eigenstates. In what follows, we refer M_2 to as

$$M_{110} = I4_1/cd + \{KI|\tfrac{1}{2}\tfrac{1}{2}0\}I4_1/cd. \tag{8}$$

3. Tetragonal Distortion of Antiferromagnetic CoO

In the tetragonally distorted crystal, the eight Co and eight O atoms in the unit cell are located at the positions

$$\begin{array}{cccc} \mathrm{Co}(000) & \mathrm{Co}(\frac{1}{2}1\frac{1}{2}) & \mathrm{Co}(1\frac{1}{2}1) & \mathrm{Co}(11\frac{1}{2}) \\ \mathrm{Co}(0\frac{1}{2}\frac{1}{2}) & \mathrm{Co}(\frac{1}{2}\frac{1}{2}0) & \mathrm{Co}(\frac{3}{2}11) & \mathrm{Co}(\frac{1}{2}\frac{1}{2}\frac{1}{2}) \end{array} \tag{9}$$

and

$$\begin{array}{cccc} \mathrm{O}(\frac{1}{4}\frac{1}{4}0) & \mathrm{O}(\frac{3}{4}\frac{5}{4}\frac{1}{2}) & \mathrm{O}(\frac{5}{4}\frac{3}{4}1) & \mathrm{O}(\frac{1}{4}\frac{1}{4}\frac{1}{2}) \\ \mathrm{O}(\frac{3}{4}\frac{3}{4}0) & \mathrm{O}(\frac{1}{4}\frac{3}{4}\frac{1}{2}) & \mathrm{O}(\frac{3}{4}\frac{5}{4}1) & \mathrm{O}(\frac{3}{4}\frac{3}{4}\frac{3}{2}), \end{array} \tag{10}$$

respectively, in the coordinate system defined by the basic translations $\boldsymbol{T}_1$, $\boldsymbol{T}_2$, and $\boldsymbol{T}_3$ of Γ_q^v given in Figure 1. The Positions 9 and 10 are the Wyckoff positions 16c and 16e (with $x = 0$) of the space group $I4_1/acd$ (142) [5]. It should be noted that the unit cell of Γ_q^v does not contain 16 Co atoms and 16 O atoms as is often assumed (and is suggested by the notations 16c and 16e of the Wyckoff positions). In the present paper, the point in the center of the tetragonal prism is not (and must not be) an additional point within the unit cell, but is a lattice point connected by translation symmetry with the other lattice points. Thus, there are 8 Co and 8 O atoms in the unit cell.

The tetragonal magnetic structure produces initially a distortion invariant under the magnetic group M_{142} in antiferromagnetic CoO. Since a system invariant under M_{142} does not possess antiferromagnetic eigenstates, the crystal must be additionally distorted in such a way that the electronic Hamiltonian still commutes with the symmetry operations of M_{110}, but does not commute with the symmetry operations of $M_{142} - M_{110}$, cf. Section 3 of [23]. The only distortion bringing the desired effect is a shift of the Co atoms in $\pm(\boldsymbol{T}_1 + \boldsymbol{T}_3)$ and $\pm(\boldsymbol{T}_2 + \boldsymbol{T}_3)$ direction from their positions 9, as indicated by the arrows in Figure 1b. In fact, the magnetic structure together with the shifts in Figure 1b is invariant under the two generating elements 4 and under the anti-unitary element $\{KI|\frac{1}{2}\frac{1}{2}0\}$ defining M_{110}, but the dislocations are not invariant under the inversion $\{I|000\}$ being a generating element of M_{142}. The oxygen atoms are not shifted from their positions 10 because any shift of the oxygen atoms would be incompatible with the magnetic group M_{110}.

This result may be understood by inspection of Figure 1, but also in terms of Wyckoff positions: the type III Shubnikov group M_{110} may be written in the form [25]

$$M_{110} = I4_1/cd + \{K|000\}\Big(G - I4_1/cd\Big) \tag{11}$$

where

$$G = I4_1/cd + \{I|\tfrac{1}{2}\tfrac{1}{2}0\}I4_1/cd \tag{12}$$

is an ordinary (unitary) space group. Equation (11) shows that the Wyckoff positions of M_{110} are equal to the Wyckoff positions of G, since the operator $\{K|000\}$ of time inversion does not influence the atomic positions. G is equivalent to the group $I4_1/acd$ (142) because we obtain the elements of G when we transform the elements of $I4_1/acd$ by the translation $\{E|\frac{1}{4}\frac{1}{4}0\}$. This statement may be demonstrated by means of the generating elements

$$\begin{aligned} \{C_{4z}^{+}|\tfrac{1}{2}00\} &= \{E|\tfrac{1}{4}\tfrac{1}{4}0\}\{C_{4z}^{+}|\tfrac{1}{2}00\}\{E|\tfrac{1}{4}\tfrac{1}{4}0\}^{-1}, \\ \{\sigma_{da}|\tfrac{1}{2}\tfrac{1}{2}0\} &= \{E|\tfrac{1}{4}\tfrac{1}{4}0\}\{\sigma_{da}|\tfrac{1}{2}\tfrac{1}{2}0\}\{E|\tfrac{1}{4}\tfrac{1}{4}0\}^{-1}, \\ \{I|\tfrac{1}{2}\tfrac{1}{2}0\} &= \{E|\tfrac{1}{4}\tfrac{1}{4}0\}\{I|000\}\{E|\tfrac{1}{4}\tfrac{1}{4}0\}^{-1}, \end{aligned} \tag{13}$$

see Equation (1.5.12) and Table 3.2 of [25]. Consequently, we receive the origin of G by shifting the origin of $I4_1/acd$ (142) about

$$\boldsymbol{t}_0 = \tfrac{1}{4}\boldsymbol{T}_1 + \tfrac{1}{4}\boldsymbol{T}_2, \tag{14}$$

that means, by shifting the origin from a Co atom to an O atom, see Figure 1. Thus, the Wyckoff positions are interchanged: In the group G and, hence, in the magnetic group M_{110}, the Co atoms lie on the position 16*e* of the group $I4_1/acd$ (142), and the O atoms on the position 16*c*. The position 16*e* contains a parameter (usually x) describing the shifts of the Co atoms indicated in Figure 1b, the O atoms on position 16*c* are fixed. This fact plays an essential role in the following Section 4.

4. Monoclinic-Like Distortion

As is the case with antiferromagnetic NiO and MnO, also antiferromagnetic CoO is clearly deformed by the magnetic structure but, additionally, by a slight distortion seemingly incompatible with the magnetic structure. In NiO [23] and MnO [22], this additional distortion is evidently produced by the oxygen atoms which form an rhombohedral-*like* array within the monoclinic magnetic group M_9 of antiferromagnetic NiO and MnO. This distortion was called "inner distortion" of the magnetic group M_9 because the symmetry of M_9 is not disturbed (and must not be disturbed) by the rhombohedral-like distortion. In CoO, on the other hand, the magnetic group M_{110} is tetragonal and the additional distortion proved experimentally to be monoclinic [8]. This can be understood as follows:

Figure 1 shows the distorted antiferromagnetic structure of CoO with the magnetic group M_{110}. The arrows in Figure 1b specify the shifts of the cobalt atoms from their positions in Equation (9). These shifts stabilize, on the one hand, the antiferromagnetic structure (Section 2) and produce, on the other hand, a strong tetragonal distortion of the crystal. Within this distortion, adjacent Co atoms are dislocated either in the same or in different directions and, consequently, their distance and, hence, their mutual attraction varies around its value in the paramagnetic state. Consequently, the crystal is tetragonally distorted in such a way that the basic translations $\boldsymbol{T}_1$, $\boldsymbol{T}_2$, and $\boldsymbol{T}_3$ of Γ_q^v are no longer embedded in the cubic lattice since this lattice no longer exists.

The oxygen atoms, on the other hand, are not shifted from their positions in the tetragonal body-centered lattice, that means, from their position given in the list 10. Thus, their mutual distances are essentially the same as in the paramagnetic phase. Just as in NiO and MnO, they form a periodic array within the lattice of the Co atoms. We assume again that this array forms a Bravais lattice, which does not contain eight O atoms, but only one O atom in the unit cell. The array of the oxygen atoms is spanned by the vectors $\boldsymbol{\rho}_1$, $\boldsymbol{\rho}_2$,

and $\boldsymbol{\rho}_3$ in Figure 2. Though these vectors are symmetry operations in the paramagnetic lattice, they are no translation operators in the tetragonal distorted crystal. Nevertheless, they give an approximate picture of the array of the oxygen atoms. In antiferromagnetic NiO and MnO, the vectors $\boldsymbol{\rho}_i$ define an rhombohedral-like array of the oxygen atoms because they form a trigonal basis within the monoclinic crystals of NiO and MnO, see Section 4 of [23]. In CoO, on the other hand, this basis is not trigonal because the vectors $\boldsymbol{\rho}_i$ have different lengths: the length of $\boldsymbol{\rho}_1$ is different from the lengths of $\boldsymbol{\rho}_2$ and $\boldsymbol{\rho}_3$ in the tetragonally deformed crystal,

$$|\boldsymbol{\rho}_1| \neq |\boldsymbol{\rho}_2| = |\boldsymbol{\rho}_3|, \tag{15}$$

if $c \neq \sqrt{2}a$ (i.e., if the crystal is no longer cubic), see Figure 2. Thus, the vectors $\boldsymbol{\rho}_i$ define a monoclinic base-centered array of the oxygen atoms, see Table 3.1 of [25]. As stated above, this array is not exactly monoclinic because the vectors $\boldsymbol{\rho}_i$ are no translational symmetry operations in the distorted crystal. Therefore, I call it a "monoclinic-like" distortion of antiferromagnetic CoO being an "inner distortion" of the magnetic group M_{110}. This will say that the monoclinic-like distortion of the oxygen atoms is not connected with any change or modification of the tetragonal symmetry of the antiferromagnetic state, which remains invariant under the symmetry operations of the magnetic group M_{110}.

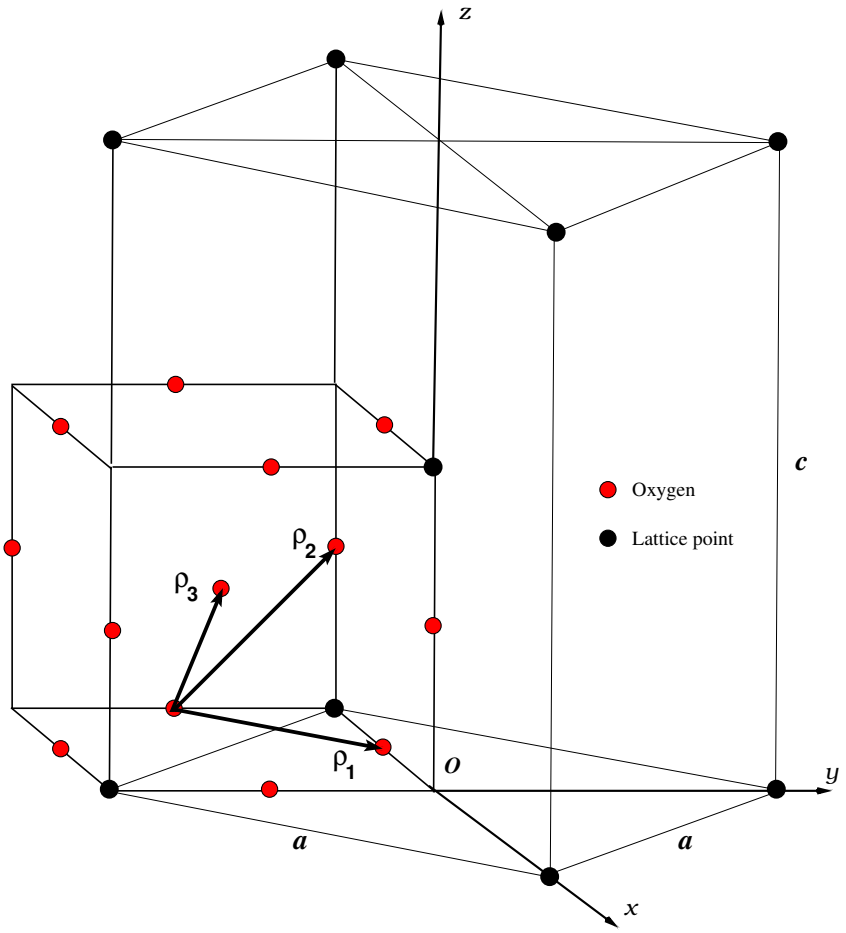

Figure 2. Oxygen atoms in the body-centered tetragonal Bravais lattice Γ_q^v. The Co atoms are not shown.

5. Application of the Non-Adiabatic Heisenberg Model

The NHM defines in narrow, partly filled electronic energy bands a strongly correlated nonadiabatic atomic-like motion. The nonadiabatic localized states defining this atomic-like motion are represented by symmetry-adapted and optimally localized Wannier functions [9]. In the following Section 5.1, we will show that the band structure of para-

magnetic CoO contains an "insulating band" [24] whose Bloch functions can be unitarily transformed into symmetry-adapted and optimally localized Wannier functions including all the electrons at the Fermi level. In the second Section 5.2 we will show that the band structure of antiferromagnetic CoO encloses two "magnetic bands" [23] related to the magnetic group M_{110} of the antiferromagnetic phase. The Bloch functions of these two bands can be unitarily transformed into optimally localized Wannier functions symmetry-adapted to M_{110}. They are even "magnetic super bands" [23] since all the electrons at the Fermi level belong to these two magnetic band.

5.1. Atomic-Like Electrons in Paramagnetic CoO

Figure 3 shows the band structure of paramagnetic CoO. The band indicated by the bold lines is characterized by Bloch functions with the symmetry:

$$\Gamma_3^+,\ L_3^+,\ X_1^+ + X_3^+,\ W_1 + W_4 \tag{16}$$

of band 5 listed Table A3a. Thus, the Bloch functions of this band can be unitarily transformed into optimally localized Wannier functions adapted to the cubic fcc symmetry and centered at the Co atoms. On the other hand, the Bloch functions cannot be unitarily transformed in such a way that the Wannier functions are centered at the O atoms since the symmetry of the Bloch functions at point L does not coincide with the symmetry of band 5 in Table A3b. The Bloch functions 16 define a band with two branches yielding two degenerate Wannier functions with Γ_3^+ symmetry at each Co atom. There symmetry may be called "d-like" since the energy band 16 originates entirely from a d orbital of Co, see Table 2.7 of [25]. If this d-like band is half-filled, it defines an atomic-like motion qualifying paramagnetic CoO to be a Mott insulator because it consists of all the branches crossing the Fermi level. In the paramagnetic system the atomic-like motion occurs solely between the Co atoms.

5.2. Atomic-Like Electrons in Antiferromagnetic CoO

Table A4 lists the only magnetic band related to the magnetic group M_{110} of antiferromagnetic CoO. Figure 4 shows the band structure of paramagnetic CoO in Figure 3 as folded into the Brillouin zone Γ_q^v of the tetragonal body-centered magnetic structure. The band highlighted in Figure 3 by the bold line (the insulating band) becomes in Figure 4 twice the magnetic band in Table A4. The Bloch functions defining the sixteen branches of these two magnetic bands are highlighted in red. They can be unitarily transformed into three types of optimally localized Wannier functions symmetry-adapted to M_{110}: Either (i) the Wannier functions are centered twice at the eight Co atoms (that means two Wannier functions are at each Co atom), or (ii) they are centered twice at the eight O atoms; or (iii) they are centered at both the eight Co atoms and at the eight O atoms.

The atomic-like motion defined by the first and the second possibility (i) and (ii) clearly has a higher Coulomb energy than the atomic-like motion belonging to the third possibility (iii) because the Coulomb repulsion between two electrons occupying localized states at the same atom is greater than the repulsion of two electrons occupying localized states at different (adjacent) atoms. Thus, the last case (iii) defines the energetically most favorable non-adiabatic atomic-like motion which stabilizes the antiferromagnetic structure with the magnetic group M_{110} [23,26]. Moreover, the two magnetic bands are magnetic super bands since they comprise all the branches crossing the Fermi level and, thus, qualify antiferromagnetic CoO to be a Mott insulator [23]. While in the paramagnetic system, the atomic-like motion occurs solely between the Co atoms (Section 5.1), it comprises in the antiferromagnetic phase both, the Co and O atoms.

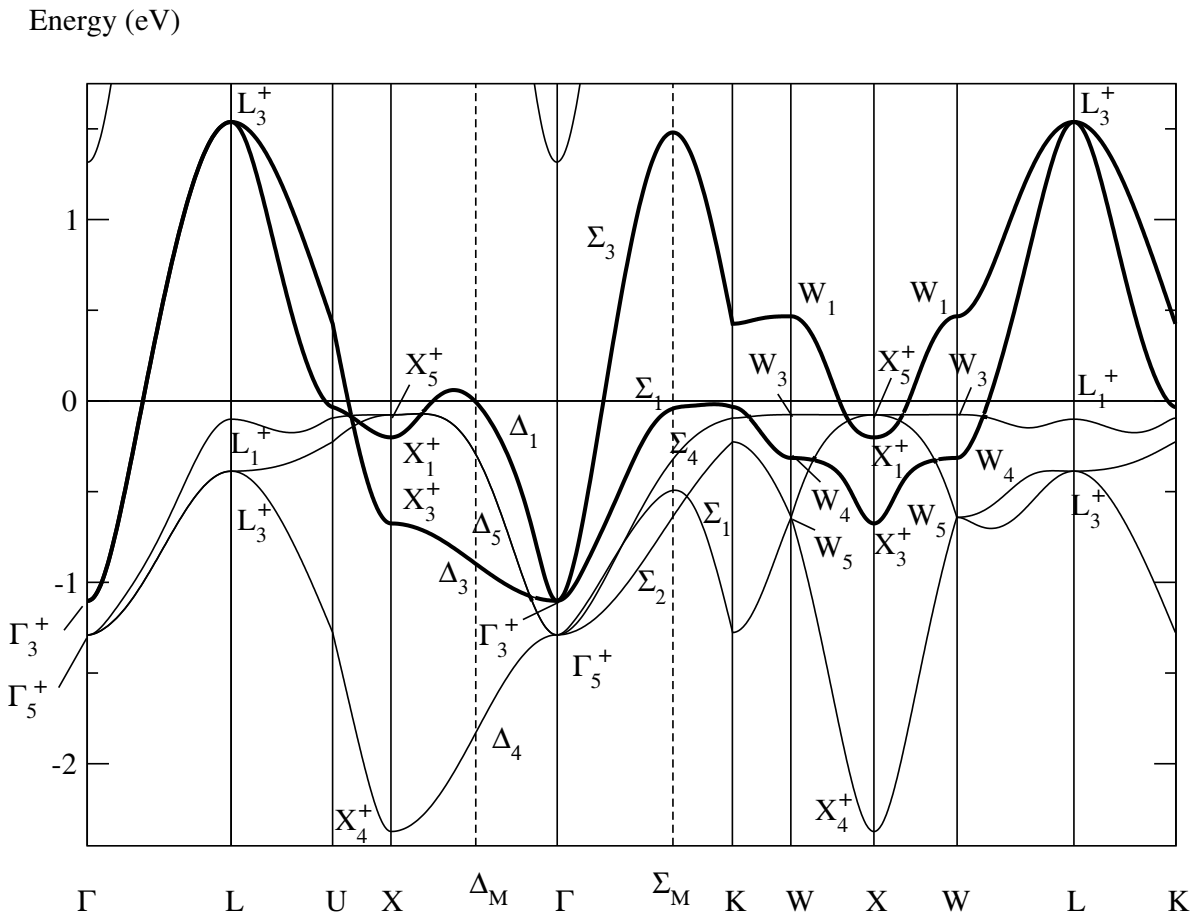

Figure 3. Conventional band structure (Section 5 of [22]) of paramagnetic fcc CoO as calculated by the FHI-aims program [10,11] using the length $a = 4.260$ Å of the paramagnetic unit cell as given in [27]. The symmetry labels as defined in Table A1 of [23] are determined by the author (as described in Section 2 of [23]), the symmetry on the lines Σ and Δ are defined by Table A6a. The notations of the points and lines of symmetry in the Brillouin zone for Γ_c^f follow Figure 3.14 of Ref. [25]. The insulating band is highlighted by the bold line.

It should be noted that we can define in the band structure of antiferromagnetic CoO other narrow bands differing (slightly) from the bands highlighted in red, but coinciding also with the symmetry of the band in Table A4. They form likewise magnetic bands if they are half-filled. It is not easy to say which bands best represent the nonadiabatic atomic-like motion in antiferromagnetic CoO. In any case, the two highlighted bands are a first approach to describing the atomic-like motion because, in this case, the localized states in antiferromagnetic CoO most resemble the localized states in the paramagnetic phase. At this stage, we realize that two magnetic bands exist, but we do not know the exact combination of their branches.

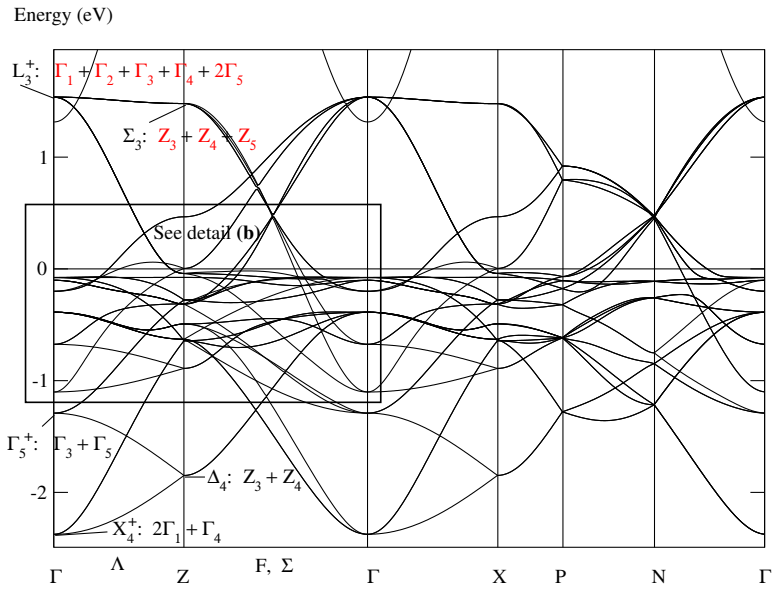

(**a**)

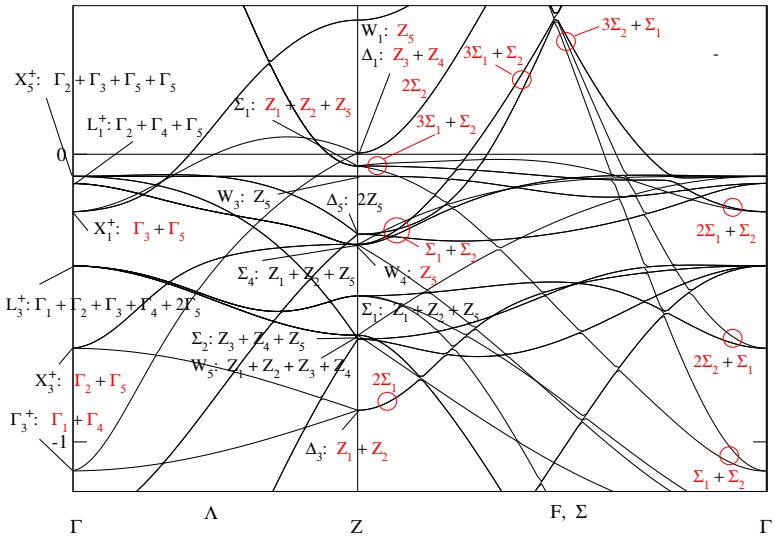

(**b**)

Figure 4. The band structure of CoO given in Figure 3 folded into the Brillouin zone for the tetragonal body-centered lattice Γ_q^v of the magnetic group M_{110}. As in Figure 3, the bands are calculated by the FHI-aims program [10,11]. At points Γ and Z, first the symmetry of the Bloch functions at the equivalent point in the fcc Brillouin zone is given. Then, after the colon, the symmetry of these Bloch functions in the tetragonal body-centered Brillouin zone is specified as given in Table A5. On the line Σ,F, the symmetry labels Σ_1 and Σ_2 are determined by Table A6b. The Bloch functions highlighted in red form two magnetic bands (i.e., twice the band in Table A4) consisting of sixteen branches assigned to the eight cobalt and eight oxygen atoms. The notations of the points and lines of symmetry follow Figure 3.10b of Ref. [25].

6. Results

Under the assumption that the non-collinear multi-spin-axis magnetic structure as proposed by van Laar is realized in antiferromagnetic CoO, essential features of CoO can be understood:

6.1. Tetragonal Distortion

The non-collinear magnetic structure is invariant under the magnetic group $M_{142} = I_c4_1/acd$ (Equation (3)). However, an electronic Hamiltonian invariant under time inversion cannot possess magnetic eigenstates (Section 2) if it commutes with all the symmetry operations of M_{142}. For this reason, the crystal is markedly tetragonally deformed (see Section 3 and Figure 1) in order that the group M_{110} in Equation (8) becomes the magnetic group of antiferromagnetic CoO.

6.2. Monoclinic-Like Distortion

This tetragonal deformation produces a monoclinic-like deformation of the array of the oxygen atoms comparable with the rhombohedral-like deformation proposed in NiO and MnO (Section 4). This monoclinic-like deformation does not influence the magnetic structure, and thus, does not modify the magnetic group M_{110}. Consequently, no inconsistency between the tetragonal and monoclinic-like distortion remains.

6.3. Magnetic Bands

In the band structure of CoO exist two magnetic bands related to M_{110} (Section 5.2). One of the two bands yields Wannier functions centered at the eight Co atoms, the other yields Wannier functions centered at the eight O atoms. In each case, the Wannier functions are optimally localized and adapted to the symmetry of the magnetic state. Thus, the electrons of this band may perform a nonadiabatic atomic-like motion lowering their nonadiabatic condensation energy ΔE (as defined in Equation (2.20) in [9]) by activating an exchange mechanism producing a magnetic structure with the magnetic group M_{110}, see the detailed substantiation in Section IV of [28].

6.4. Mott Insulation in the Antiferromagnetic Phase

The two magnetic bands are magnetic super bands because they comprise all the branches crossing the Fermi level. Thus, they qualify antiferromagnetic CoO to be a Mott insulator (Section 5.2). The nonadiabatic atomic-like motion involves both, the Co and the O atoms.

6.5. Mott Insulation in the Paramagnetic Phase

Independently of the special magnetic symmetry, it was shown in Section 5.1 that there exists an insulating band [23] in the paramagnetic band structure of CoO. The electrons of this band may perform a nonadiabatic atomic-like motion that qualifies CoO to be a Mott insulator also in the paramagnetic phase. The related optimally localized Wannier functions are adapted to the cubic fcc symmetry of paramagnetic CoO, are centered on the Co atoms, are twofold degenerate and have d-like Γ_3^+ symmetry. The atomic-like motion occurs exclusively between the Co atoms.

7. Discussion

7.1. Foundations of the Theory

The results of the present paper provide strong evidence that the tetragonal non-collinear multi-spin-axis structure exists in CoO. The foundations of the presented theory are the non-adiabatic Heisenberg model (NHM) [9], and the group-theoretical theorem, stating that in a system invariant under time inversion, any magnetic eigenstate and its time-inverted state belong to a two-dimensional irreducible co-representation of the magnetic group (Condition 1 in [23]).

The NHM applies group theoretical methods to the exact non-adiabatic atomic-like motion of the electrons at the Fermi level and confirms that a magnetic structure with the magnetic group M_{110} given in Equation (8) may exist in CoO. Thus, it provides the basis for any localized picture in antiferromagnetic CoO, such as for the proven concepts of correlation effects in narrow *d* bands as mentioned in Section 1.1.

7.2. Suggested Experimental Investigations

Figure 1 gives a precise prediction of the distortion of antiferromagnetic CoO. It should be possible to determine experimentally the shifts of the cobalt atoms in the same way as Goodwin et al. [29] succeeded in determining the shifts of the atoms in MnO.

The atomic-like motion in the paramagnetic phase differs from this motion in the antiferromagnetic phase: while the atomic-like motion is predicted to occur solely between the cobalt atoms in the paramagnetic phase, it involves both the cobalt and oxygen atoms in the antiferromagnetic phase. It should be possible to confirm this striking behavior experimentally.

The experimentally observed small monoclinic-like distortion of CoO in the antiferromagnetic phase is proposed to be a distortion of the array of the oxygen atoms without the involvement of the cobalt atoms (which stay tetragonally distorted), see Section 4. I believe that it should be possible to confirm also this special feature of CoO experimentally.

Funding: This publication was supported by the Open Access Publishing Fund of the University of Stuttgart.

Acknowledgments: I am much indebted to Guido Schmitz for his continuing support of my work.

Conflicts of Interest: The author declares no conflict of interest.

Abbreviations

The following abbreviations are used in this manuscript:

NHM	Non-adiabatic Heisenberg model
E	Identity operation
I	Inversion
C_{4z}^{+}	anti-clockwise rotation through 90° about the z axis
C_{2a}	Rotation through 180° as indicated in Figure 1
σ_{da}	Reflection IC_{2a}
K	anti-unitary operator of time inversion

Appendix A. Group-Theoretical Tables

This appendix provides Tables A1–A6 along with notes to the tables.

Table A1. Character tables of the single valued irreducible representations of the tetragonal body-centered space group $I4_1/acd = \Gamma_q^v D_{4h}^{20}$ (142).

	Γ(000)					
	$\{K\|000\}$	$\{E\|000\}$	$\{C_{2z}\|\frac{1}{2}0\frac{1}{2}\}$	$\{C_{4z}^{-}\|\frac{1}{2}\frac{1}{2}\frac{1}{2}\}$ $\{C_{4z}^{+}\|\frac{1}{2}00\}$	$\{C_{2b}\|0\frac{1}{2}\frac{1}{2}\}$ $\{C_{2a}\|\frac{1}{2}\frac{1}{2}0\}$	$\{C_{2x}\|00\frac{1}{2}\}$ $\{C_{2y}\|0\frac{1}{2}0\}$
Γ_1^+	(a)	1	1	1	1	1
Γ_2^+	(a)	1	1	1	−1	−1
Γ_3^+	(a)	1	1	−1	1	−1
Γ_4^+	(a)	1	1	−1	−1	1
Γ_5^+	(a)	2	−2	0	0	0
Γ_1^-	(a)	1	1	1	1	1
Γ_2^-	(a)	1	1	1	−1	−1
Γ_3^-	(a)	1	1	−1	1	−1
Γ_4^-	(a)	1	1	−1	−1	1
Γ_5^-	(a)	2	−2	0	0	0

Table A1. *Cont.*

	Γ(000)					
	$\{I\|000\}$	$\{\sigma_z\|\frac{1}{2}0\frac{1}{2}\}$	$\{S_{4z}^{+}\|\frac{1}{2}\frac{1}{2}\frac{1}{2}\}$ $\{S_{4z}^{-}\|\frac{1}{2}00\}$	$\{\sigma_{db}\|0\frac{1}{2}\frac{1}{2}\}$ $\{\sigma_{da}\|\frac{1}{2}\frac{1}{2}0\}$	$\{\sigma_x\|00\frac{1}{2}\}$ $\{\sigma_y\|0\frac{1}{2}0\}$
Γ_1^+	1	1	1	1	1
Γ_2^+	1	1	1	−1	−1
Γ_3^+	1	1	−1	1	−1
Γ_4^+	1	1	−1	−1	1
Γ_5^+	2	−2	0	0	0
Γ_1^-	−1	−1	−1	−1	−1
Γ_2^-	−1	−1	−1	1	1
Γ_3^-	−1	−1	1	−1	1
Γ_4^-	−1	−1	1	1	−1
Γ_5^-	−2	2	0	0	0

	$Z(\frac{1}{2}\frac{1}{2}\overline{\frac{1}{2}})$						
	$\{E\|000\}$	$\{E\|001\}$	$\{C_{2z}\|\frac{1}{2}0\frac{3}{2}\}$	$\{C_{2z}\|\frac{1}{2}0\frac{1}{2}\}$	$\{C_{2a}\|\frac{1}{2}\frac{1}{2}1\}$ $\{C_{2b}\|0\frac{1}{2}\frac{3}{2}\}$	$\{C_{2a}\|\frac{1}{2}\frac{1}{2}0\}$ $\{C_{2b}\|0\frac{1}{2}1\}$	$\{I\|000\}$ $\{I\|001\}$
Z_1	2	−2	2	−2	2	−2	0
Z_2	2	−2	−2	2	0	0	0
Z_3	2	−2	2	−2	−2	2	0
Z_4	2	−2	−2	2	0	0	0

	$Z(\frac{1}{2}\frac{1}{2}\overline{\frac{1}{2}})$ *(continued)*						
	$\{\sigma_z\|\frac{1}{2}0\frac{1}{2}\}$ $\{\sigma_z\|\frac{1}{2}0\frac{3}{2}\}$	$\{\sigma_{db}\|0\frac{1}{2}\frac{1}{2}\}$ $\{\sigma_{da}\|\frac{1}{2}\frac{3}{2}0\}$	$\{\sigma_{db}\|0\frac{1}{2}\frac{3}{2}\}$ $\{\sigma_{da}\|\frac{1}{2}\frac{1}{2}0\}$	$\{C_{2y}\|0\frac{3}{2}0\}$ $\{C_{2y}\|0\frac{1}{2}0\}$ $\{C_{2x}\|00\frac{3}{2}\}$ $\{C_{2x}\|00\frac{1}{2}\}$	$\{C_{4z}^{+}\|\frac{1}{2}01\}$ $\{C_{4z}^{-}\|\frac{1}{2}\frac{1}{2}\frac{1}{2}\}$ $\{C_{4z}^{-}\|\frac{1}{2}\frac{1}{2}\frac{3}{2}\}$ $\{C_{4z}^{+}\|\frac{1}{2}00\}$	$\{\sigma_y\|0\frac{1}{2}0\}$ $\{\sigma_y\|0\frac{1}{2}1\}$ $\{\sigma_x\|00\frac{3}{2}\}$ $\{\sigma_x\|00\frac{1}{2}\}$	$\{S_{4z}^{-}\|\frac{1}{2}00\}$ $\{S_{4z}^{+}\|\frac{1}{2}\frac{1}{2}\frac{1}{2}\}$ $\{S_{4z}^{+}\|\frac{1}{2}\frac{1}{2}\frac{3}{2}\}$ $\{S_{4z}^{-}\|\frac{1}{2}10\}$
Z_1	0	0	0	0	0	0	0
Z_2	0	2	−2	0	0	0	0
Z_3	0	0	0	0	0	0	0
Z_4	0	−2	2	0	0	0	0

Notes to Table A1:

(i) The notations of the points of symmetry follow Figure 3.10b of [25].
(ii) Only the two points of symmetry Γ and Z invariant under the complete space group are listed.
(iii) The character tables are determined from Table 5.7 in [25].
(iv) K denotes the operator of time inversion. The entry (a) is determined by Equation (7.3.51) of [25] and indicates that the related co-representations of the magnetic group $I4_1/acd + \{K|000\}I4_1/acd$ follow Case (a) as defined in Equation (7.3.45) of [25].

Table A2. Character tables of the single valued irreducible representations of the tetragonal body-centered space group $I4_1/cd = \Gamma_q^v C_{4v}^{12}$ (110).

Γ(000)								
	$\{K\|000\}$	$\{KI\|\frac{1}{2}\frac{1}{2}0\}$	$\{K\|\frac{1}{2}\frac{1}{2}0\}$	$\{E\|000\}$	$\{C_{2z}\|\frac{1}{2}0\frac{1}{2}\}$	$\{C_{4z}^-\|\frac{1}{2}\frac{1}{2}\frac{1}{2}\}$ $\{C_{4z}^+\|\frac{1}{2}00\}$	$\{\sigma_{da}\|\frac{1}{2}\frac{1}{2}0\}$ $\{\sigma_{db}\|0\frac{1}{2}\frac{1}{2}\}$	$\{\sigma_y\|0\frac{1}{2}0\}$ $\{\sigma_x\|00\frac{1}{2}\}$
Γ_1	(a)	(a)	(a)	1	1	1	1	1
Γ_2	(a)	(a)	(a)	1	1	1	−1	−1
Γ_3	(a)	(a)	(a)	1	1	−1	1	−1
Γ_4	(a)	(a)	(a)	1	1	−1	−1	1
Γ_5	(a)	(a)	(a)	2	−2	0	0	0

$Z(\frac{1}{2}\frac{1}{2}\overline{\frac{1}{2}})$							
	$\{K\|000\}$	$\{KI\|\frac{1}{2}\frac{1}{2}0\}$	$\{K\|\frac{1}{2}\frac{1}{2}0\}$	$\{E\|000\}$	$\{C_{2z}\|\frac{1}{2}0\frac{1}{2}\}$	$\{C_{2z}\|\frac{1}{2}0\frac{3}{2}\}$	$\{E\|100\}$
Z_1	(c)	(a)	(c)	1	1	−1	−1
Z_2	(c)	(a)	(c)	1	1	−1	−1
Z_3	(c)	(a)	(c)	1	1	−1	−1
Z_4	(c)	(a)	(c)	1	1	−1	−1
Z_5	(a)	(a)	(a)	2	−2	2	−2

$Z(\frac{1}{2}\frac{1}{2}\overline{\frac{1}{2}})$ *(continued)*						
	$\{\sigma_{db}\|0\frac{1}{2}\frac{3}{2}\}$ $\{\sigma_{da}\|\frac{1}{2}\frac{1}{2}0\}$	$\{\sigma_{da}\|\frac{1}{2}\frac{1}{2}1\}$ $\{\sigma_{db}\|0\frac{1}{2}\frac{1}{2}\}$	$\{C_{4z}^-\|\frac{1}{2}\frac{1}{2}\frac{1}{2}\}$ $\{C_{4z}^+\|\frac{1}{2}00\}$	$\{C_{4z}^+\|\frac{1}{2}01\}$ $\{C_{4z}^-\|\frac{1}{2}\frac{1}{2}\frac{3}{2}\}$	$\{\sigma_x\|00\frac{1}{2}\}$ $\{\sigma_y\|0\frac{1}{2}1\}$	$\{\sigma_y\|0\frac{1}{2}0\}$ $\{\sigma_x\|00\frac{3}{2}\}$
Z_1	1	−1	i	−i	i	−i
Z_2	1	−1	−i	i	−i	i
Z_3	−1	1	−i	i	i	−i
Z_4	−1	1	i	−i	−i	i
Z_5	0	0	0	0	0	0

$P(\frac{1}{4}\frac{1}{4}\frac{1}{4})$				
	$\{E\|000\}$	$\{E\|010\}$	$\{E\|020\}$	$\{E\|030\}$
P_1	2	−2i	−2	2i

$P(\frac{1}{4}\frac{1}{4}\frac{1}{4})$ *(continued)*						
	$\{\sigma_y\|0\frac{3}{2}1\}$ $\{\sigma_y\|0\frac{1}{2}0\}$	$\{\sigma_y\|1\frac{3}{2}1\}$ $\{\sigma_y\|0\frac{1}{2}1\}$	$\{C_{2z}\|\frac{1}{2}0\frac{1}{2}\}$ $\{C_{2z}\|\frac{1}{2}1\frac{3}{2}\}$	$\{C_{2z}\|\frac{1}{2}0\frac{3}{2}\}$ $\{C_{2z}\|\frac{3}{2}1\frac{3}{2}\}$	$\{\sigma_x\|00\frac{7}{2}\}$ $\{\sigma_x\|00\frac{3}{2}\}$	$\{\sigma_x\|00\frac{1}{2}\}$ $\{\sigma_x\|01\frac{3}{2}\}$
P_1	0	0	0	0	0	0

$N(0\frac{1}{2}0)$				
	$\{E\|000\}$	$\{\sigma_{db}\|0\frac{1}{2}\frac{1}{2}\}$	$\{E\|010\}$	$\{\sigma_{db}\|0\frac{3}{2}\frac{1}{2}\}$
N_1	1	i	−1	−i
N_2	1	−i	−1	i

$X(00\frac{1}{2})$					
	$\{E\|000\}$	$\{E\|001\}$	$\{\sigma_x\|00\frac{3}{2}\}$ $\{\sigma_x\|00\frac{1}{2}\}$	$\{C_{2z}\|\frac{1}{2}0\frac{1}{2}\}$ $\{C_{2z}\|\frac{1}{2}0\frac{3}{2}\}$	$\{\sigma_y\|0\frac{1}{2}1\}$ $\{\sigma_y\|0\frac{1}{2}0\}$
X_1	2	−2	0	0	0

Notes to Table A2:

(i) The notations of the points of symmetry follow Figure 3.10b of [25].
(ii) The character tables are determined from Table 5.7 in [25].
(iii) K denotes the operator of time inversion. The entries (a) and (c) are determined by Equation (7.3.51) of [25]. They indicate whether the related co-representations of

the magnetic groups $I4_1/cd + \{K|000\}I4_1/cd$, $I4_1/cd + \{KI|\frac{1}{2}\frac{1}{2}0\}I4_1/cd$, and $I4_1/cd + \{K|\frac{1}{2}\frac{1}{2}0\}I4_1/cd$ follow Case (a) or Case (c) as defined in Equations (7.3.45) and (7.3.47), respectively, of [25].

Table A3. Excerpt of Table 1 of [24] showing only Band 5 with optimally localized Wannier functions of Γ_3^+ symmetry centered at the Co atoms (Table (**a**)) and the O atoms (Table (**b**)).

(**a**)	Co(000)	Γ	*X*	*L*	*W*
Band 5	Γ_3^+	Γ_3^+	$X_1^+ + X_3^+$	L_3^+	$W_1 + W_4$
(**b**)	$O(\bar{\frac{1}{2}}\frac{1}{2}\frac{1}{2})$	Γ	*X*	*L*	*W*
Band 5	Γ_3^+	Γ_3^+	$X_1^+ + X_3^+$	L_3^-	$W_1 + W_4$

Table A4. Symmetry labels of the Bloch functions at the points of symmetry in the Brillouin zone for $I4_1/cd$ (110) of the only energy band with symmetry-adapted and optimally localized Wannier functions centered at the Co (Table (**a**)) as well as O (Table (**b**)) atoms, respectively.

(**a**)	**Co**	Co(000)	Co($\frac{1}{2}1\frac{1}{2}$)	Co($1\frac{1}{2}1$)	Co($11\frac{1}{2}$)	Co($0\frac{1}{2}\frac{1}{2}$)	Co($\frac{1}{2}\frac{1}{2}0$)	Co($\frac{3}{2}11$)	Co($\frac{1}{2}\frac{1}{2}\frac{1}{2}$)
(**b**)	**O**	O($\frac{1}{4}\frac{1}{4}0$)	O($\frac{3}{4}\frac{5}{4}\frac{1}{2}$)	O($\frac{5}{4}\frac{3}{4}1$)	O($\frac{1}{4}\frac{1}{4}\frac{1}{2}$)	O($\frac{3}{4}\frac{3}{4}0$)	O($\frac{1}{4}\frac{3}{4}\frac{1}{2}$)	O($\frac{3}{4}\frac{5}{4}1$)	O($\frac{3}{4}\frac{3}{4}\frac{3}{2}$)
		$\boldsymbol{d}_1$	$\boldsymbol{d}_1$	$\boldsymbol{d}_1$	$\boldsymbol{d}_1$	$\boldsymbol{d}_1$	$\boldsymbol{d}_1$	$\boldsymbol{d}_1$	$\boldsymbol{d}_1$
(**a**)	(**b**)	$\{KI\|\frac{1}{2}\frac{1}{2}0\}$	Γ		*Z*		*N*	*X*	*P*
		OK	$\Gamma_1 + \Gamma_2 + \Gamma_3 + \Gamma_4 + 2\Gamma_5$		$Z_1 + Z_2 + Z_3 + Z_4 + 2Z_5$		$4N_1 + 4N_2$	$4X_1$	$4P_1$

Notes to Table A4

(i) The symmetry of the band related to the Co atoms in Table (**a**) coincides fully with the symmetry of the band related to the O atoms in Table (**b**).
(ii) The notations of the points of symmetry in the Brillouin zone for Γ_q^v follow Figure 3.10b of [25] and the symmetry notations of the Bloch functions are defined in Table A2.
(iii) The bands are determined following Theorem 5 of [30].
(iv) The point groups G_{0Co} and G_{0O} of the positions [30] of the Co and the O atoms contain only the identity operation:

$$G_{0Co} = G_{0O} = \Big\{\{E|\mathbf{0}\}\Big\}. \tag{A1}$$

Thus, the Wannier functions at the atoms belong to the simple representation

	$\{E\|\mathbf{0}\}$
$\boldsymbol{d}_1$	1

of G_{0Co} and G_{0O}.
(v) The table defines a band consisting of eight branches with Bloch functions that can be unitarily transformed into Wannier functions being:

- As well localized as possible;
- Centered at the eight Co atoms (**a**) or at the eight O atoms (**b**); and
- Symmetry adapted to the unitary subgroup $I4_1/cd$ (110) of the magnetic group M_{110}. In the present case, this means that the symmetry operations of $I4_1/cd$ effect an interchange of the eight Wannier functions in the unit cell, cf. note (xi) of Table A2 in [23].
- The entry "OK" indicates that the Wannier functions follow not only Theorem 5, but also Theorem 7 of [30]. Consequently, they may be chosen symmetry-adapted to the complete magnetic group M_{110}, cf. note (xii) of Table A2 in [23].

Table A5. Compatibility relations between the Brillouin zone for the fcc space group $Fm3m$ (225) of paramagnetic CoO and the Brillouin zone for the space group $I4_1/cd$ (110) of the antiferromagnetic structure in distorted CoO.

$\mathbf{\Gamma(000)}$									
Γ_1^+ Γ_1	Γ_2^+ Γ_4	Γ_2^- Γ_3	Γ_1^- Γ_2	Γ_3^+ $\Gamma_1+\Gamma_4$	Γ_3^- $\Gamma_2+\Gamma_3$	Γ_4^+ $\Gamma_2+\Gamma_5$	Γ_5^+ $\Gamma_3+\Gamma_5$	Γ_4^- $\Gamma_1+\Gamma_5$	Γ_5^- $\Gamma_4+\Gamma_5$
$X(\frac{1}{2}0\frac{1}{2})$									
X_1^+ $\Gamma_3+\Gamma_5$	X_2^+ $\Gamma_1+2\Gamma_4$	X_3^+ $\Gamma_2+\Gamma_5$	X_4^+ $2\Gamma_1+\Gamma_4$	X_5^+ $\Gamma_2+\Gamma_3+2\Gamma_5$	X_1^- $\Gamma_4+\Gamma_5$	X_2^- $\Gamma_2+2\Gamma_3$	X_3^- $\Gamma_1+\Gamma_5$	X_4^- $2\Gamma_2+\Gamma_3$	X_5^- $\Gamma_1+\Gamma_4+2\Gamma_5$
$L(\frac{1}{2}\frac{1}{2}\frac{1}{2})$									
L_1^+ $\Gamma_2+\Gamma_4+\Gamma_5$	L_2^+ $\Gamma_1+\Gamma_3+\Gamma_5$	L_1^- $\Gamma_1+\Gamma_3+\Gamma_5$	L_2^- $\Gamma_2+\Gamma_4+\Gamma_5$	L_3^+ $\Gamma_1+\Gamma_2+\Gamma_3+\Gamma_4+2\Gamma_5$				L_3^- $\Gamma_1+\Gamma_2+\Gamma_3+\Gamma_4+2\Gamma_5$	
$\Sigma_M(\frac{1}{4}\frac{1}{4}\frac{1}{2})$									
Σ_1 $Z_1+Z_2+Z_5$		Σ_2 $Z_3+Z_4+Z_5$		Σ_3 $Z_3+Z_4+Z_5$				Σ_4 $Z_1+Z_2+Z_5$	
$W''(\frac{1}{4}\overline{\frac{1}{4}\frac{1}{2}})$									
W_1 Z_5		W_2 Z_5		W_3 Z_5		W_4 Z_5		W_5 $Z_1+Z_2+Z_3+Z_4$	
$\Delta'_M(\overline{\frac{1}{4}\frac{1}{4}}0)$									
Δ_1 Z_3+Z_4		Δ_2 Z_1+Z_2		Δ_3 Z_1+Z_2		Δ_4 Z_3+Z_4		Δ_5 $2Z_5$	
$\Delta_M(\frac{1}{4}0\frac{1}{4})$									
Δ_1 X_1		Δ_2 X_1		Δ_3 X_1		Δ_4 X_1		Δ_5 $2X_1$	
$\Lambda_M(\frac{1}{4}\frac{1}{4}\frac{1}{4})$									
Λ_1 N_1+N_2				Λ_2 N_1+N_2				Λ_3 $2N_1+2N_2$	
$W'(\overline{\frac{3}{4}\frac{1}{2}\frac{1}{4}})$									
W_1 X_1		W_2 X_1		W_3 X_1		W_4 X_1		W_5 $2X_1$	

Notes to Table A5:

(i) The upper rows list the representations of the little groups of the points of symmetry in the Brillouin zone for $Fm3m$, and the lower rows list representations of the little groups of the related points of symmetry in the Brillouin zone for $I4_1/cd$.
The representations in the same column are compatible in the following sense: Bloch functions that are basis functions of a representation $\boldsymbol{D}_i$ in the upper row can be unitarily transformed into the basis functions of the representation given below $\boldsymbol{D}_i$.
(ii) The notations of the points of symmetry follow Figures 3.14 and 3.10 (b), respectively, of [25].
(iii) The notations of the representations are defined in Table A4 of [23] and Table A2, respectively.
(iv) The compatibility relations are determined as described in great detail in [31].

Table A6. Compatibility relations between points and lines in the Brillouin zone for the fcc space group $Fm3m$ (225) of paramagnetic CoO (Table (**a**)) and in the Brillouin zone for the space group $I4_1/cd$ (110) of the antiferromagnetic structure of distorted CoO (Table (**b**)), as far as the are useful for an understanding of Figures 3 and 4.

Γ(000)									
Γ_1^+ Δ_1	Γ_2^+ Δ_3	Γ_2^- Δ_4	Γ_1^- Δ_2	Γ_3^+ $\Delta_1 + \Delta_3$	Γ_3^- $\Delta_2 + \Delta_4$	Γ_4^+ $\Delta_2 + \Delta_5$	Γ_5^+ $\Delta_4 + \Delta_5$	Γ_4^- $\Delta_1 + \Delta_5$	Γ_5^- $\Delta_3 + \Delta_5$
$\Gamma(000)$									
Γ_1^+ Σ_1	Γ_2^+ Σ_3	Γ_2^- Σ_4	Γ_1^- Σ_2	Γ_3^+ $\Sigma_1 + \Sigma_3$	Γ_3^- $\Sigma_2 + \Sigma_4$	Γ_4^+ $\Sigma_2 + \Sigma_3 + \Sigma_4$	Γ_5^+ $\Sigma_1 + \Sigma_2 + \Sigma_4$	Γ_4^- $\Sigma_1 + \Sigma_3 + \Sigma_4$	Γ_5^- $\Sigma_1 + \Sigma_2 + \Sigma_3$
$X(\frac{1}{2}0\frac{1}{2})$									
X_1^+ Δ_1	X_2^+ Δ_2	X_3^+ Δ_3	X_4^+ Δ_4	X_5^+ Δ_5	X_1^- Δ_2	X_2^- Δ_1	X_3^- Δ_4	X_4^- Δ_3	X_5^- Δ_5
(**a**)									

Γ(010), Γ(000)				
Γ_1 F_1, Σ_1	Γ_2 F_2, Σ_2	Γ_3 F_1, Σ_1	Γ_4 F_2, Σ_2	Γ_5 $F_1 + F_2, \Sigma_1 + \Sigma_2$
$Z(\frac{1}{2}\frac{1}{2}\frac{\overline{1}}{2})$				
Z_1 F_1	Z_2 F_1	Z_3 F_2	Z_4 F_2	Z_5 $F_1 + F_2$
$\Gamma(000)$				
Γ_1 Λ_1	Γ_2 Λ_2	Γ_3 Λ_3	Γ_4 Λ_4	Γ_5 Λ_5
$Z(\frac{1}{2}\frac{1}{2}\frac{\overline{1}}{2})$				
Z_1 Λ_4	Z_2 Λ_2	Z_3 Λ_1	Z_4 Λ_3	Z_5 Λ_5
(**b**)				

References

1. Rooksby, H. A note on the structure of nickel oxide at subnormal and elevated temperatures. *Acta Crystallogr.* **1948**, *1*, 226. [CrossRef]
2. Shull, C.G.; Strauser, W.A.; Wollan, E.O. Neutron Diffraction by Paramagnetic and Antiferromagnetic Substances. *Phys. Rev.* **1951**, *83*, 333–345. [CrossRef]
3. Roth, W.L. Magnetic Structures of MnO, FeO, CoO, and NiO. *Phys. Rev.* **1958**, *110*, 1333–1341. [CrossRef]
4. Cracknell, A.P.; Joshua, S.J. The space group corepresentations of antiferromagnetic NiO. *Math. Proc. Camb. Philos. Soc.* **1969**, *66*, 493–504. [CrossRef]
5. van Laar, B. Multi-Spin-Axis Structure for CoO. *Phys. Rev.* **1965**, *138*, A584–A587. [CrossRef]
6. Timm, L.; Tucker, M.G.; Keen, D.A.; Thygesen, P.M.M.; Saines, P.J.; Goodwin, A.L. Exploration of antiferromagnetic CoO and NiO using reverse Monte Carlo total neutron scattering refinements. *Phys. Scr.* **2016**, *91*, 114004. [CrossRef]
7. Tomiyasu, K.; Inami, T.; Ikeda, N. Magnetic structure of CoO studied by neutron and synchrotron x-ray diffraction. *Phys. Rev. B* **2004**, *70*, 184411. [CrossRef]
8. Jauch, W.; Reehuis, M.; Bleif, H.J.; Kubanek, F.; Pattison, P. Crystallographic symmetry and magnetic structure of CoO. *Phys. Rev. B* **2001**, *64*, 052102. [CrossRef]
9. Krüger, E. Non-adiabatic extension of the Heisenberg model. *Phys. Rev. B* **2001**, *63*, 144403–144413. [CrossRef]
10. Blum, V.; Gehrke, R.; Hanke, F.; Havu, P.; Havu, V.; Ren, X.; Reuter, K.; Scheffler, M. Ab initio molecular simulations with numeric atom-centered orbitals. *Comput. Phys. Commun.* **2009**, *180*, 2175–2196. [CrossRef]
11. Havu, V.; Blum, V.; Havu, P.; Scheffler, M. Efficient O(N)O(N) integration for all-electron electronic structure calculation using numeric basis functions. *Comput. Phys. Commun.* **2009**, *228*, 8367–8379. [CrossRef]
12. Austin, I.G.; Mott, N.F. Metallic and Nonmetallic Behavior in Transition Metal Oxides. *Science* **1970**, *168*, 71–77. [CrossRef] [PubMed]

13. Mott, N.F. On the transition to metallic conduction in semiconductors. *Can. J. Phys.* **1956**, *34*, 1356–1368. [CrossRef]
14. Mott, N.F. The transition to the metallic state. *Philos. Mag.* **1961**, *6*, 287–309. [CrossRef]
15. Mott, N.F. The Basis of the Electron Theory of Metals, with Special Reference to the Transition Metals. *Proc. Phys. Soc. Sect.* **1949**, *62*, 416–422. [CrossRef]
16. Gavriliuk, A.G.; Trojan, I.A.; Struzhkin, V.V. Insulator-Metal Transition in Highly Compressed NiO. *Phys. Rev. Lett.* **2012**, *109*, 086402. [CrossRef]
17. Trimarchi, G.; Wang, Z.; Zunger, A. Polymorphous band structure model of gapping in the antiferromagnetic and paramagnetic phases of the Mott insulators MnO, FeO, CoO, and NiO. *Phys. Rev. B* **2018**, *97*, 035107. [CrossRef]
18. Dalverny, A.L.; Filhol, J.S.; Lemoigno, F.; Doublet, M.L. Interplay between Magnetic and Orbital Ordering in the Strongly Correlated Cobalt Oxide: A DFT U Study. *J. Phys. Chem.* **2010**, *114*, 21750–21756. [CrossRef]
19. Zhang, Y.; Furness, J.; Zhang, R.; Wang, Z.; Zunger, A.; Sun, J. Symmetry-breaking polymorphous descriptions for correlated materials without interelectronic U. *Phys. Rev. B* **2020**, *102*, 045112. [CrossRef]
20. Lanatà, N.; Lee, T.H.; Yao, Y.X.; Stevanović, V.; Dobrosavljević, V. Connection between Mott physics and crystal structure in a series of transition metal binary compounds. *NPJ Comput. Mater.* **2019**, *5*, 30. [CrossRef]
21. Gillen, R.; Robertson, J. Accurate screened exchange band structures for the transition metal monoxides MnO, FeO, CoO and NiO. *J. Phys. Condens. Matter* **2013**, *25*, 165502. [CrossRef]
22. Krüger, E. Nonadiabatic Atomic-Like State Stabilizing Antiferromagnetism and Mott Insulation in MnO. *Symmetry* **2020**, *12*, 1913. [CrossRef]
23. Krüger, E. Structural Distortion Stabilizing the Antiferromagnetic and Insulating Ground State of NiO. *Symmetry* **2019**, *12*, 56. [CrossRef]
24. Krüger, E. Wannier States of FCC Symmetry Qualifying Paramagnetic NiO to Be a Mott Insulator. *Symmetry* **2020**, *12*, 687. [CrossRef]
25. Bradley, C.; Cracknell, A.P. *The Mathematical Theory of Symmetry in Solids*; Claredon: Oxford, UK, 1972.
26. Krüger, E. Stability and symmetry of the spin-density-wave-state in chromium. *Phys. Rev. B* **1989**, *40*, 11090–11103. [CrossRef]
27. Bredow, T.; Gerson, A.R. Effect of exchange and correlation on bulk properties of MgO, NiO, and CoO. *Phys. Rev. B* **2000**, *61*, 5194–5201. [CrossRef]
28. Krüger, E. Energy band with Wannier functions of ferromagnetic symmetry as the cause of ferromagnetism in iron. *Phys. Rev. B* **1999**, *59*, 13795–13805. [CrossRef]
29. Goodwin, A.L.; Tucker, M.G.; Dove, M.T.; Keen, D.A. Magnetic Structure of MnO at 10 K from Total Neutron Scattering Data. *Phys. Rev. Lett.* **2006**, *96*, 047209. [CrossRef] [PubMed]
30. Krüger, E.; Strunk, H.P. Group Theory of Wannier Functions Providing the Basis for a Deeper Understanding of Magnetism and Superconductivity. *Symmetry* **2015**, *7*, 561–598. [CrossRef]
31. Krüger, E. Symmetry of Bloch functions in the space group D_{4h}^{6} of perfect antiferromagnetic chromium. *Phys. Rev. B* **1985**, *32*, 7493–7501. [CrossRef] [PubMed]